Structural Chemistry (2019) 30:369–384
https://doi.org/10.1007/s11224-018-1210-5

ORIGINAL RESEARCH

Molecular dynamics assessment of doxorubicin–carbon nanotubes molecular interactions for the design of drug delivery systems

M. Leonor Contreras[1] · Camila Torres[2] · Ignacio Villarroel[2] · Roberto Rozas[1]

Received: 23 July 2018 / Accepted: 17 October 2018 / Published online: 29 October 2018

Abstract

Carbon nanotubes (CNTs) constitute an interesting material for nanomedicine applications because of their unique properties, especially their ability to penetrate membranes, to transport drugs specifically and to be easily functionalized. In this work, the energies of the intermolecular interactions of single-walled CNTs and the anticancer drug doxorubicin (DOX) were determined using the AMBER 12 molecular dynamics MM/PBSA and MM/GBSA methods with the aim of better understanding how the structural parameters of the nanotube can improve the interactions with the drug and to determine which structural parameters are more important for increasing the stability of the complexes formed between the CNTs and DOX. The a*rmchair*, *zigzag*, and *chiral* nanotubes were finite hydrogen-terminated open tubes, and the DOX was encapsulated inside the tube or adsorbed on the nanotube surface. Pentagon/heptagon bumpy defects and polyethylene glycol (PEG) nanotube functionalization were also studied. The best interaction occurred when the drug was located inside the cavity of the nanotube. *Armchair* and *zigzag* nanotubes doped with nitrogen, favored interaction with the drug, whereas *chiral* nanotubes exhibited better drug interactions when having bumpy defects. The π-π stacking and N-H…π electrostatic interactions were important components of the attractive drug-nanotube forces, enabling significant flattening of the nanotube to favor a dual strong interaction with the encapsulated drug, with DOX–CNT equilibrium distances of 3.1–3.9 Å. These results can contribute to the modeling of new drug-nanotube delivery systems.

Keywords Bumpy nanotubes · Nitrogen-doped carbon nanotubes · Doxorubicin encapsulation · Drug delivery system · Interaction energies · Noncovalent interactions · π-π stacking

Electronic supplementary material The online version of this article (https://doi.org/10.1007/s11224-018-1210-5) contains supplementary material, which is available to authorized users.

✉ M. Leonor Contreras
leonor.contreras@usach.cl

Camila Torres
camila.torresv@usach.cl

Ignacio Villarroel
gatrevolution@gmail.com

Roberto Rozas
roberto.rozas@usach.cl

[1] Laboratorio de Química Computacional y Propiedad Intelectual, Departamento de Ciencias del Ambiente, Facultad de Química y Biología, Universidad de Santiago de Chile, USACH, Avenida Libertador Bernardo O'Higgins 3363, Casilla 40, Correo 33, Santiago, Chile

[2] Departamento de Computación e Informática, Facultad de Ingeniería, Universidad de Santiago de Chile, USACH, Avenida Ecuador 3659, Santiago, Chile

Introduction

Carbon nanotubes (CNTs) are compounds with broad potential applications in biology and biomedicine [1–4]. Several reviews on CNTs address the characterization and release of bioactives [5] and the design of drug delivery systems [6]. The functionalization of nanotubes with several fragments in a simultaneous way allows their use for targeting, imaging, and therapy [7]. For all these systems, the solubility of CNTs is a crucial parameter because little soluble CNTs have been shown to cause macrophage secretion of proinflammatory cytokines [8]. Appropriate functionalization reactions [9–11] have been necessary to solve some problems with the solubility and toxicity of nanotubes [8, 12, 13]. For instance, polyethylene glycol, PEG, has been used for increasing CNT solubility [14]. When CNTs solubility, concentration, and purity are controlled, they are shown to be non-toxic [13]. Nitrogen functionalization of nanotubes also makes them less toxic [15] and provides important catalytic properties [16–18], which

motivated nitrogen-doped CNTs to be studied as a hydrogen storage material [19–21].

Doxorubicin (DOX) is an effective neoplastic agent [22–27] that presents a moderate toxicity [28]; however, the FDA (Food and Drug Administration) has approved its use [29]. DOX adsorption on suitably functionalized CNTs decreases its toxicity and increases its bioavailability [11, 30].

Within applications in biomedicine, for a systematic approach with minimal risk to patients, a detailed molecular-level understanding is required to reduce the potential for adverse effects. From this perspective, computer simulation is a good initial step prior to chemical synthesis and clinical research.

Among the methods of computational evaluation performed prior to the experimental development of a drug and its transportation to the target in the body, several computational alternatives have been implemented considering CNTs and DOX [31–34]. In the search of modeling drug delivery systems based on nanotubes and DOX, it is important to know the effect of nanotube chirality and nitrogen doping, and also the effect of the presence of structural defects and groups that enhance the solubility of nanotubes on noncovalent drug-receptor molecular interactions. To the best of our knowledge, there is no systematic research on this topic for the mentioned molecular system. Also, there is not known data showing the effect that certain structural features of nanotubes, for example, five- and seven-membered cyclic units (which produce structures known as bumpy nanotubes), can produce on the drugs transporting. These types of defects can modify the conductive properties of nanotubes that have been considered as new materials of interest in the nanoelectronics industry [35, 36].

In this work, DOX–CNT interaction energies determined through molecular dynamics methods for CNTs of different chirality, including nitrogen-doped, bumpy-type defects and PEG groups, are systematically studied with the aim of finding a kind of ranking of CNT ability to get associated with DOX as a contribution to the knowledge of molecular drug-CNT interactions, which constitute a critical stage of evaluation in the design of better drug delivery systems.

Our results reveal that *armchair*, *chiral*, and *zigzag* CNTs exhibit optimal drug-nanotube interactions at a single fixed diameter despite that *chiral* CNTs exhibit the best ability to encapsulate DOX. It is found also that bumpy defects and PEG fragments in *chiral* CNTs enhance DOX encapsulation; CNT diameter has a more relevant effect than length; CNT chirality governs nitrogen-doping effect.

Simulation methods

The DOX–CNT complexes were prepared using Hypertube [37] and HyperChem [38] in Windows. The nanotubes were all open, single-walled, and hydrogen terminated. Files were saved as *pdb* and *mol2* format using the OpenBabel program (version 2.1.1, C. Morley, 2006). Then, a home-made automation program in Linux built the 19 new files needed to proceed with the molecular dynamics Assisted Model Building with Energy Refinement (AMBER) simulations [39], as shown in Fig. 1. The ligand in all cases was DOX (see Fig. 2). Ligand-receptor complexes initially contain DOX adsorbed either at an edge of the nanotube, on the nanotube outer surface (called DoxOut) or encapsulated inside the nanotube (called DoxIn), as shown in Fig. 3 (*a* and *b*). The created files include: the AMBER *pdb* files (which have a different format than the Babel *pdb* files) for (i) the receptor (CNT); (ii) the ligand (DOX), and (iii) the CNT–DOX complex, as well as the *setype* and *setcharge* files for each of the three systems. In addition, *xleap* files for the three systems and for the complex solvated with the TIP3P water model in a 10.0 Å octahedral box were created. All used the Bondi radius. These files and the files mentioned above enable the generation of the *prmtop* and *inpcrd* files necessary for running molecular dynamics simulations. Special care was taken with the overall net charge of the receptor, and when necessary, the *setcharge* files for the complex and the receptor were manually corrected until the total net charge was zero, as verified by the *xleap* process. Ligand charges were obtained from the HF/6-31G(d) optimized geometry. For verification purposes, some of the calculations were performed with the Restrained ElectroStatic Potential (RESP) charges [40], obtained by means of AMBER antechamber. In *xleap* mode, the molecular structure of the system was visualized before the simulation, which helped to prevent mistakes (for instance, erroneous formation of a DOX–CNT covalent bond).

Molecular dynamics simulations were conducted using the combined AMBER ff99SB and GAFF force fields (some missing parameters were manually entered through a frcntn.frcmod file as shown in Table S2). They were performed using five sequential steps: (1) minimization (at constant volume and using a small restriction); (2) heating from 0.0 to 300.0 K (at constant volume, with a small restriction); (3) density equilibrium (at constant temperature and pressure, with a small restriction); (4) equilibrium (at constant pressure, without restriction and with a different random number seed); and (5) production (at constant pressure). Previous work on specialized analysis and comparison of yields concluded that more accurate binding energy values are obtained when the production stage consists of several short independent stages [41]. In the present work, 50 ps of heating, 50 ps of density, 500 ps of equilibrium, and six stages of 250 ps each for the production step were used (coordinates were recorded every 10 ps), yielding a total of 2.1 ns of molecular dynamics simulation time. For verification, 4 ns, 8 ns, and 9.8 ns periods were run for a couple of files using 12, 24, and 35 independent stages of 250 ps each, respectively. Also, 40 ns and 100 ns

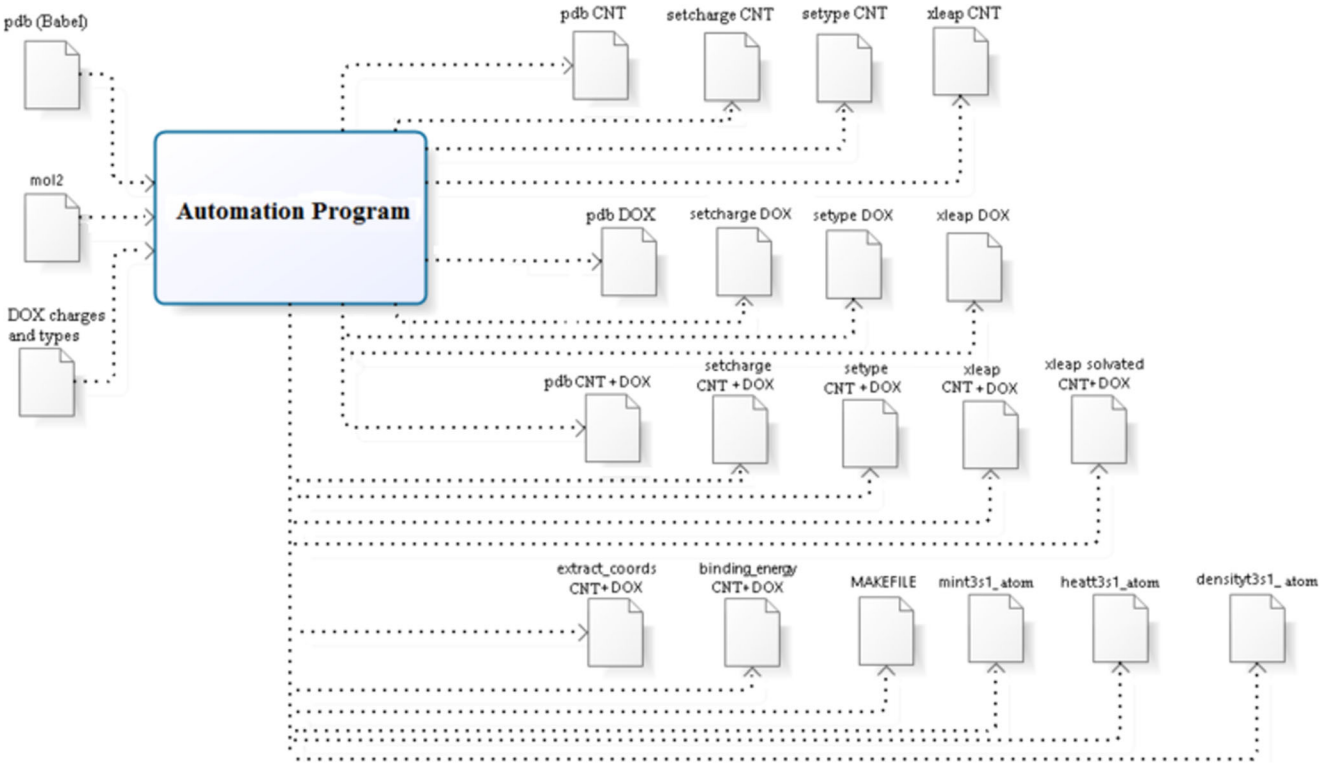

Fig. 1 Automation program scheme showing the 19 files generated to run one DOX–CNT binding energy calculation using the MM/PBSA and MM/GBSA methods of AMBER

periods were run for a couple of files using independent stages of 5 ns each. Free energy calculations using the MM/PBSA and MM/GBSA approaches were performed according to expression (1):

$$\Delta G = \langle G_{NTC-DOX} - G_{NTC} - G_{DOX} \rangle_{NTC-DOX} \quad (1)$$

where $G_{NTC\text{-}DOX}$, G_{NTC}, and G_{DOX} correspond to the Gibbs free energy terms for the complex, receptor and ligand, respectively. Each of these terms is obtained using expression (2):

$$G = E_{bond} + E_{el} + E_{vdW} + E_{pol} + E_{np} - TS \quad (2)$$

where E_{bond} (bond, angle, dihedral), E_{el} (electrostatic), E_{vdW} (van der Waals) are the standard molecular mechanics (MM) energy terms, E_{pol} (polar term) is calculated by solving the Poisson-Boltzmann (PB) and/or generalized Born (GB) equation, E_{np} (non-polar term) is estimated from a linear relation with the solvent accessible surface area (SA), T is the absolute temperature and S is the entropy term estimated through a normal-mode analysis of the vibrational frequencies.

The assumption that no significant conformational changes occur upon binding is used so that the snapshots for all three species can be obtained from a single trajectory. This approach is more efficient and provides more accurate results than the use of three independent trajectories [41]. For the extraction of the final coordinates, 200 frames of the production stage were used. The results were visualized using the virtual molecular dynamics (VMD) program (http://www.ks.uiuc.edu/Research/vmd/).

Results and discussion

This section presents and discusses the noncovalent nanotube-drug interaction energy results obtained for CNTs of different diameters, length, and chirality, some of them being nitrogen doped. The presence of bumpy defects and a number of PEG substitutions was also considered.

The ligand-receptor binding energies for DOX and *zigzag*, *chiral* and *armchair* nanotubes with comparable diameters and lengths under both the Poisson-Boltzmann (PB) and the Generalized Born (GB) approaches are presented in Table 1. Results analysis will be based only on the PB values since the PB and GB binding energies, are not significantly different for equivalent systems, and exhibit the same complex stability trends, although these energies are not the real binding energies because their calculation does not consider the (unfavorable) translational and rotational entropy term. However, these binding energies are informative in terms of the relative values for the different nanotube structures, as shown below. Although the structural parameters are strongly related, effort is made to present the results for each parameter/effect independently.

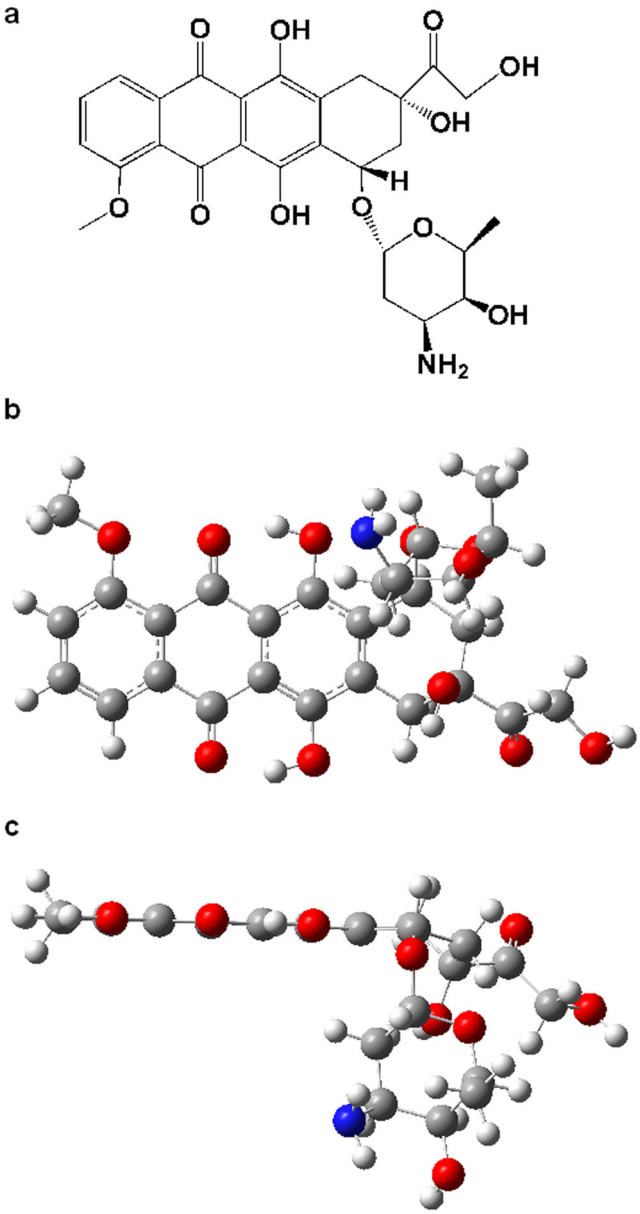

Fig. 2 Representations of the DOX structure ($C_{27}H_{29}NO_{11}$). **a** DOX molecular formula; **b** optimized DOX frontal view; **c** optimized DOX lateral view

Chirality effect

The results suggest that the DOX–CNT binding energy is significantly dependent on the chirality of the nanotube, as shown in Table 1 for nanotubes of similar size with diameters of 15.4–16.3 Å and lengths of 18.3–20.9 Å (diameters and lengths correspond to the initial MM+ optimized nanotube geometries). *Chiral* CNTs exhibit stronger drug-nanotube interactions than *zigzag* and *armchair* CNTs, with favorable PB binding energy differences of 27 and 29 kcal/mol, respectively. The PB value for the *chiral* DOX–CNT complex is − 105 kcal/mol (run 14), compared with − 78.2 and − 75.6 kcal/mol for the complexes formed with *zigzag* and *armchair* nanotubes, respectively (runs 9 and 5). A DFT study performed using M05-2X functionals for noncovalent complexes of adsorbed DOX with closed *armchair* (5,5) and *zigzag* (10,0) nanotubes found the same trend: *zigzag* nanotubes form slightly more stable complexes with DOX than *armchair* nanotubes [23].

Nitrogen doping effect

The presence of four nitrogen atoms on nanotubes, equivalent to having two pyrimidine rings, strengthens DOX–CNT interaction for *zigzag* and *armchair* nanotubes. PB binding energy differences with the corresponding undoped nanotubes of 9.4 and 32.8 kcal/mol are obtained, with PB energy values of − 87.6 and − 108.4 kcal/mol for the doped *zigzag* and *armchair* nanotubes (runs 10 and 6, Table 1), respectively, compared with PB values of − 78.2 and − 75.6 kcal/mol for undoped systems (runs 9 and 5, respectively). After increasing the nitrogen content to eight nitrogen atoms in the nanotube, less significant PB energy differences with the corresponding undoped systems are obtained (3.3 and 1.3 kcal/mol for *zigzag* and *armchair* nanotubes, respectively (runs 11 and 7), compared with runs 9 and 5 in Table 1). The same favorable trend is observed for *armchair* nanotubes with a smaller diameter (14 Å). In addition to the nitrogen content, the DOX–CNT binding energy also depends on the distribution of the nitrogen atoms in the nanotube since when the nitrogen atoms are located along the axial axis of the nanotube (run 3), the effect is less favorable than when they are arranged in the transverse form (run 2), with PB energies of − 102.1 and − 109.8 kcal/mol, respectively.

Nitrogen-doped *chiral* nanotubes exhibit different behavior. Nitrogen doping with four nitrogen atoms in this case does not significantly favor DOX–CNT interactions, with a PB energy of − 105.3 kcal/mol (run 15), compared with − 105.0 kcal/mol for the undoped system (run 14). The complex formed with nanotubes with eight nitrogen atoms exhibits a PB energy of − 76.4 kcal/mol (run 16). The same effect is observed when *chiral* nanotubes are functionalized with PEG fragments (two PEG fragments of eight ethylene glycol units each), where nitrogen does not favor the DOX–CNT interaction (run 19 vs run 18).

As expected, the systems with the strongest DOX–CNT interaction exhibit smaller equilibrium distances between the encapsulated doxorubicin planar hydroxyanthraquinone rings and the nanotube sidewall ($d_{p\text{-}NT}$) due to the known π-π stacking interaction. This interaction is very important, as is the contribution of the other electrostatic interactions (i.e., CH…π, OH…π, CO…π, NH… π), as many authors have reported, some based on DOX fluorescence determinations [30, 31, 42, 43]. For instance, from the four *armchair* (10,10) nanotubes listed in Table 1, the two systems with smaller PB energy values (runs 2 and 3) exhibit smaller $d_{p\text{-}}$

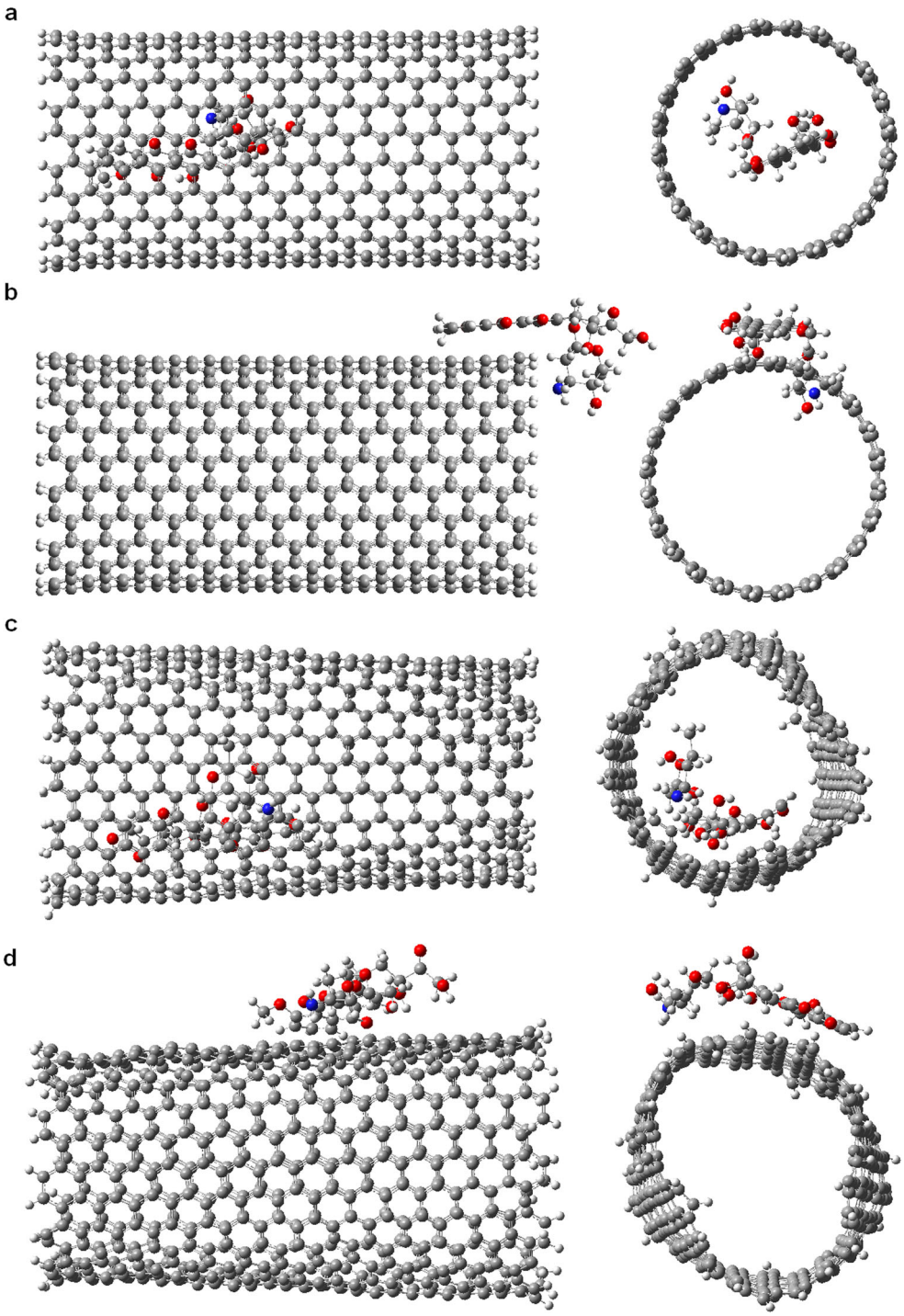

Fig. 3 Representation of the complex structures for encapsulation (DoxIn) and adsorption (DoxOut) of DOX in *armchair* CNTs, before and after the AMBER simulation. **a** Initial A(12,12)DoxIn; **b** initial A(12,12)DoxOut; **c** final A(12,12)DoxIn; **d** final A(12,12)DoxOut

$_{NT}$, and the two systems with larger PB energy values (runs 1 and 4) exhibit larger values of $d_{p\text{-}NT}$. The same behavior is observed for *armchair* (12,12) nanotubes doped with four nitrogen atoms (run 6), which have a PB binding energy of − 108.4 kcal/mol and a $d_{p\text{-}NT}$ of 3.312 Å. Meanwhile, the corresponding undoped system (run 5), with a PB binding energy of − 75.6 kcal/mol, exhibits a $d_{p\text{-}NT}$ of 3.475 Å. *Zigzag* and *chiral* nanotubes do not follow the same trend, with the exception of PEG-functionalized *chiral* nanotubes (runs 18 and 19), where the system with the strongest DOX–CNT interaction (− 105.9 kcal/mol, run 18) exhibits a smaller value of $d_{p\text{-}NT}$ (3.346 Å).

The equilibrium distance between the encapsulated DOX-nitrogen atom and the nearest nanotube-sidewall carbon atom, $d_{N\text{-}NT}$, remains less than 3.8 Å for all the studied cases, indicating the importance of the NH…π electrostatic

interaction, especially for encapsulated systems. A different situation occurs when DOX is adsorbed instead of encapsulated. Adsorbed DOX on the external surface of a (20,0) *zigzag* nanotube (run 8) exhibits the largest $d_{N\text{-}NT}$ value in Table 1 (~ 3.8 Å) and the smallest $d_{p\text{-}NT}$ of ~ 3.2 Å with the largest PB binding energy (− 42.0 kcal/mol). NCI-plot representation [44] of the intermolecular DOX–CNT noncovalent interactions of this adsorption complex, Z(20,0)DoxOut, after the production steps of AMBER simulation, is depicted in Fig. 4 (only intermolecular interactions are considered) and validates the explained results. This is not an isolated case, as will be discussed later. The results suggest that adsorbed DOX is free to accommodate itself on the nanotube external surface, and in this situation, the π-π stacking interaction prevails over the NH…π electrostatic interaction. The contribution of the NH…π electrostatic interaction in adsorbed DOX–CNT complexes is less important than in the encapsulation complexes. A molecular dynamics simulation study of DOX–single-walled CNT complexes reported distances from the DOX center of mass to the nearest carbon atom of the CNT of 4.0 Å and 4.5 Å, for adsorption and encapsulation, respectively, both seem to be larger distances than that found in the present work and show an inverse trend [34].

For longer nanotubes, the effect of nitrogen doping is smaller and chirality dependent. *Zigzag* doped nanotubes exhibit a slightly favored DOX–CNT interaction, with PB energy of − 81.7 kcal/mol, compared with the PB energy of − 76.7 kcal/mol, for the undoped system (run 37 vs run 35, Table 2). Meanwhile, for *armchair* nanotubes, nitrogen doping does not have a significant influence on the binding energies (runs 11 and 12, Table 2), and *chiral* doped nanotubes exhibit a slightly disfavored effect (runs 21 and 22, Table 2).

Diameter and length

The smaller diameter *armchair* (10,10) nanotube complex, with a PB binding energy value of − 90.5 kcal/mol (14 Å, run 1, Table 1), exhibits a stronger DOX–CNT interaction than the corresponding larger diameter *armchair* (12,12) nanotube, with a PB value of − 75.6 kcal/mol (16.2 Å, run 5). This trend is also observed for nanotubes with a larger length. The longer a*rmchair* (10,10) nanotube complex (− 109.3 kcal/mol, run 1, Table 2) presents a stronger DOX–CNT interaction than the larger diameter *armchair* (12,12) nanotube (− 75.0 kcal/mol, run 10). This diameter trend of *armchair* nanotube complexes of different lengths is in

Table 1 The values of the binding energies for doxorubicin-nanotube complexes calculated using the Poisson-Boltzmann (PB) and Generalized Bond (GB) methods. D is the nanotube diameter, $d_{p\text{-}NT}$ is the equilibrium distance between the doxorubicin planar fragment and the nanotube sidewall surface, $d'_{p\text{-}NT}$ is the equilibrium distance between the same point of the doxorubicin planar fragment and the opposite nanotube sidewall surface, and $d_{N\text{-}NT}$ is the equilibrium distance between the doxorubicin-nitrogen atom and the nanotube sidewall surface

Run	Type	PB (kcal/mol)	GB (kcal/mol)	D (Å)	Length (Å)	$d_{p\text{-}NT}$ (Å)	$d_{N\text{-}NT}$ (Å)	$d'_{p\text{-}NT}$ (Å)
1	A(10,10)DoxIn	− 90.5	− 91.9	14.03	20.22	3.790	3.134	
2	A(10,10)4NDoxIn	− 109.8	− 114.9	14.03	20.22	3.577	3.324	3.977
3	A(10,10)4NeDoxIn	− 102.1	− 105.4	14.07	20.25	3.542	3.048	3.729
4	A(10,10)8NDoxIn	− 95.6	− 98.8	14.03	20.22	3.713	3.466	
5	A(12,12)DoxIn	− 75.6	− 75.2	16.23	20.92	3.475	3.423	
6	A(12,12)4NDoxIn	− 108.4	− 113.0	16.28	20.87	3.312	3.906	3.509
7	A(12,12)8NDoxIn	− 76.9	− 77.3	16.28	20.88	3.477	3.355	
8	Z(20,0)DoxOut	− 42.0	− 41.0	15.39	18.99	3.194	3.799	
9	Z(20,0)DoxIn	− 78.2	− 78.3	15.39	19.01	3.549	3.190	
10	Z(20,0)4NDoxIn	− 87.6	− 86.7	15.40	19.00	3.601	3.354	
11	Z(20,0)8NDoxIn	− 81.5	− 81.8	15.50	19.01	3.401	3.260	
12	Z(30,0)DoxIn	− 67.0	− 66.8	24.20	20.58	3.623	3.257	
13	Ch(12,9)DoxIn	− 110.6	− 115.2	14.00	20.31	3.680	3.164	3.844
14	Ch(13,10)DoxIn	− 105.0	− 109.5	15.50	18.33	3.750	3.793	3.896
15	Ch(13,10)4NDoxIn	− 105.3	− 110.4	15.54	18.33	3.437	3.669	4.190
16	Ch 13,10)8NDoxIn	− 76.4	− 77.2	15.50	18.33	3.466	3.693	
17	Ch(13,10)DoxIn-4PEG4.v2	− 91.1	− 91.3	16.28	19.09	3.663	3.083	
18	Ch(13,10)DoxIn-2PEG8.v2	− 105.9	− 110.4	16.13	19.08	3.346	3.796	3.545
19	Ch(13,10)4NDoxIn-2PEG8.v2	− 79.3	− 79.2	16.14	19.05	3.651	3.302	

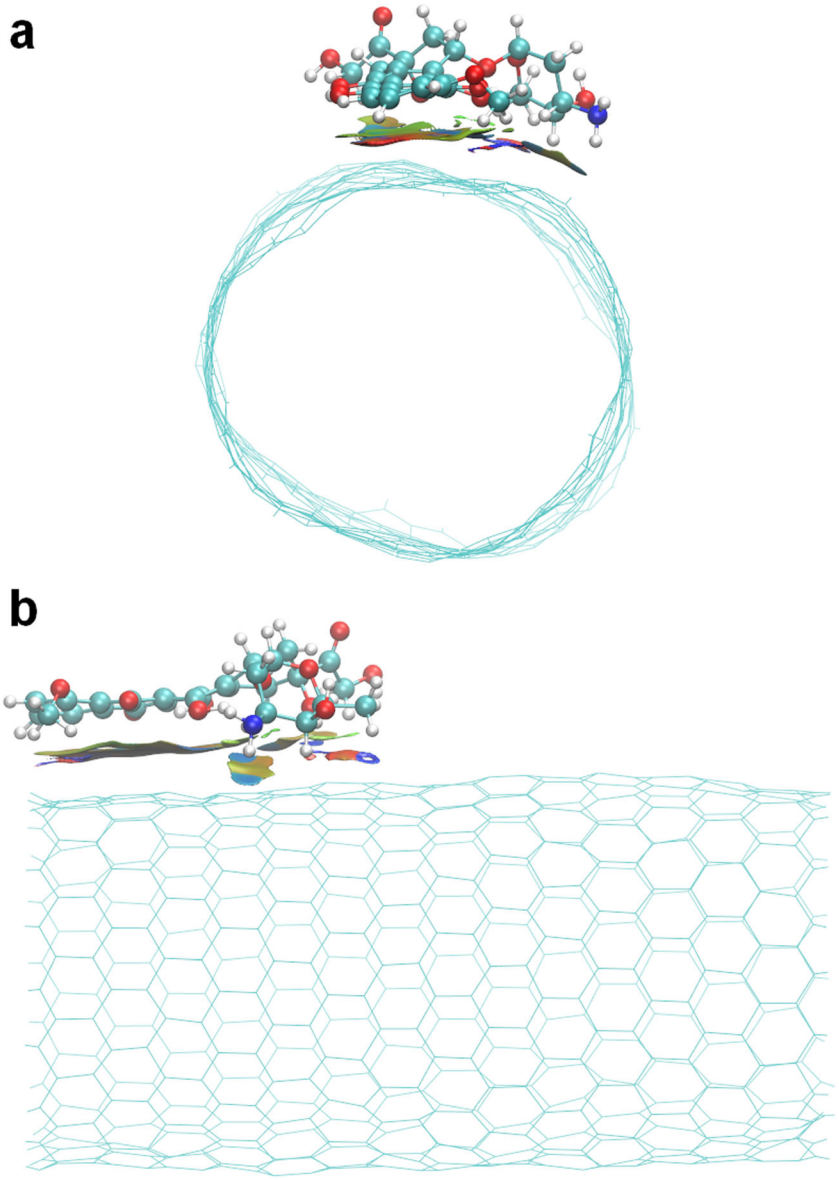

Fig. 4 Representation of the DOX–CNT noncovalent interactions for the adsorption complex Z(20,0)DoxOut after the AMBER simulation. Intermolecular 0.9; cutoff 0.01. **a** Frontal view; **b** lateral view

agreement with the reported results for DOX encapsulation with *armchair* DOX–CNT complexes using theoretical methods at the level of the hybrid meta-GGA functionals M05-2x and M06-2x [31]. Wang and Xu [31] found a diameter of 11 Å as the onset for encapsulation of DOX in *armchair* nanotubes, with 14 Å being the optimal diameter for DOX encapsulation. For diameters between 12 and 18 Å, they reported encapsulation binding energies between − 51.6 and − 53.7 kcal/mol and adsorption binding energies between − 28 and − 32 kcal/mol. Experimental DOX adsorption binding energies of − 11.5 to − 14.1 kcal/mol (− 48 to − 59 kJ/mol) were estimated for complexes of *zigzag* nanotubes of 13 to 19 Å diameter in water [43]. The results obtained in the present work, although overestimated, show good relative trends for both DOX adsorption and encapsulation binding energies to nanotubes of different chirality (with coherent equilibrium distances). Our results exhibit also good relative diameter trends, and good relative activity of *zigzag* vs *armchair* nanotubes, in agreement with reported experimental and theoretical estimations as was explained before. It is expected that considering the appropriate translational and rotational entropy terms together with the use of the Restrained ElectroStatic Potential (RESP) charges for the interacting fragments could result in more realistic drug-nanotube interaction energy values. However, that would involve a huge computational cost. In this work, when using RESP charges for DOX, calculations performed for the encapsulation of DOX in *armchair*, *chiral*, and *zigzag* nanotubes, including the adsorption of DOX in *zigzag* nanotubes, reveal indeed higher values of drug-nanotube interaction energies, as

Table 2 The values of the binding energies for doxorubicin-nanotube complexes calculated using the Poisson-Boltzmann (PB) and Generalized Bond (GB) methods. D1 and D2 are the nanotube diameters in the regular and defected parts, respectively, $d_{p\text{-}NT}$ is the equilibrium distance between the doxorubicin planar fragment and the nanotube sidewall surface, $d'_{p\text{-}NT}$ is the equilibrium distance between the same point of the doxorubicin planar fragment and the opposite nanotube sidewall surface, and $d_{N\text{-}NT}$ is the equilibrium distance between the doxorubicin-nitrogen atom and the nanotube sidewall surface

Run	Type	PB (kcal/mol)	GB (kcal/mol)	D1 (Å)	D2 (Å)	Length (Å)	$d_{p\text{-}NT}$ (Å)	$d_{N\text{-}NT}$ (Å)	$d'_{p\text{-}NT}$ (Å)
1	A(10,10)DoxIn.v1	− 109.3	− 113.2	14.04	–	34.12	3.597	3.387	3.967
2	A(10,10)DoxIn.v2	− 89.7	− 90.5	14.08	–	34.13	3.665	3.090	
3	A(10,10)4NDoxIn.v1	− 90.3	− 91.2	14.04	–	34.16	3.740	4.052	
4	A(10,10)4N'DoxIn.v1	− 109.0	− 113.6	14.04	–	34.16	3.646	3.296	3.727
5	A(10,10)BDoxDIn.v1	− 87.8	− 88.4	13.49	16.58	32.34	4.110	3.714	
6	A(10,10)BDoxDIn.v2	− 82.4	− 84.0	13.44	16.66	32.34	3.738	3.069	
7	A(10,10)BDoxRIn.v1	− 86.5	− 86.9	13.49	16.57	32.34	3.929	3.302	
8	A(10,10)BDoxRIn.v2	− 95.9	− 97.3	13.47	16.71	32.34	3.657	3.069	
9	A(12,12)DoxOut	− 43.2	− 42.0	16.03	–	32.67	3.455	3.392	
10	A(12,12)DoxIn.v1	− 75.0	− 74.1	16.04	–	32.67	3.847	2.940	
11	A(12,12)DoxIn.v2	− 77.7	− 76.7	16.01	–	32.67	3.536	3.500	
12	A(12,12)4NDoxIn.v2	− 77.0	− 76.5	16.01	–	32.67	3.389	4.116	
13	A(12,12)BDoxDIn.v1	− 73.5	− 73.3	16.02	19.97	32.28	3.966	3.483	
14	A(12,12)BDoxDIn.v2	− 66.9	− 69.9	16.11	19.78	32.26	3.782	4.398	
15	A(12,12)BDoxRIn.v1	− 72.8	− 72.7	16.06	19.92	32.20	3.798	3.277	
16	A(12,12)BDoxRIn.v2	− 77.5	− 76.8	16.83	20.09	33.76	3.882	3.753	
17	Ch(12,9)DoxIn.v1	− 85.9	− 85.9	14.00	–	33.90	3.816	3.312	
18	Ch(12,9)DoxIn.v2	− 83.7	− 84.3	14.00	–	33.90	3.573	3.460	
19	Ch(13,10)DoxOut	− 42.4	− 41.2	16.20	–	34.29	3.394	3.638	
20	Ch(13,10)DoxIn.v1	− 79.8	− 79.2	16.20	–	34.28	3.266	3.325	
21	Ch(13,10)DoxIn.v2	− 81.2	− 81.2	16.22	–	34.29	3.745	4.545	
22	Ch(13,10)4NDoxIn.v2	− 77.3	− 77.0	16.24	–	34.31	3.758	3.934	
23	Ch(13,10)BDoxR.v1	− 94.2	− 94.4	16.34	19.43	31.90	3.503	3.692	
24	Ch(13,10)BDoxR.v2	− 97.9	− 100.0	15.53	18.77	31.19	3.461	3.825	4.019
25	Ch(13,10)BDoxD.v1	− 84.1	− 85.5	16.21	19.58	33.18	3.989	3.786	
26	Ch(13,10)BDoxD.v2	− 91.5	− 92.9	16.37	19.53	33.18	3.624	3.784	
27	Ch(13,10)DoxIn-2PEG8.v2	− 92.4	− 93.3	16.24	–	32.83	3.605	3.426	
28	Ch(13,10)BDoxR-2PEG8.v2	− 84.1	− 85.0	16.09	18.86	32.23	3.675	5.474	
29	Ch(13,10)BDoxR-4PEG4.v1	− 96.7	− 98.2	16.39	20.41	32.16	3.645	3.684	
30	Ch(13,10)BDoxR-4PEG4.v2	− 83.3	− 85.7	16.39	20.41	32.16	3.660	3.641	
31	Ch(20,10)DoxIn	− 65.4	− 64.7	21.42	–	33.27	3.874	5.370	
32	Z(18,0)DoxIn.v1	− 108.5	− 113.4	14.42	–	32.97	3.465	3.404	3.955
33	Z(18,0)DoxIn.v2	− 83.8	− 84.3	14.42	–	32.97	3.465	3.447	
34	Z(20,0)DoxOut	− 43.3	− 42.1	16.21	–	31.43	3.670	4.277	
35	Z(20,0)DoxIn.v2	− 76.7	− 76.7	16.21	–	31.44	3.976	3.635	
36	Z(20,0)4NDoxIn.v1	− 78.6	− 79.8	15.64	–	30.34	3.432	3.296	
37	Z(20,0)4NDoxIn.v2	− 81.7	− 80.7	14.54	–	30.34	3.630	4.868	
38	Z(30,0)DoxOut	− 43.8	− 43.0	24.33	–	33.79	3.426	3.941	
39	Z(30,0)DoxIn	− 69.1	− 68.3	24.33	–	33.79	3.877	3.716	

expected. In addition, an excellent correlation with the respective drug-nanotube interaction energy values calculated without RESP charges was found, as seen in Fig. 5 and Table 3 which indirectly validates the found CNT ranking of DOX association ability. The particular values of the DOX Mulliken and RESP atomic charges are shown in Table S1

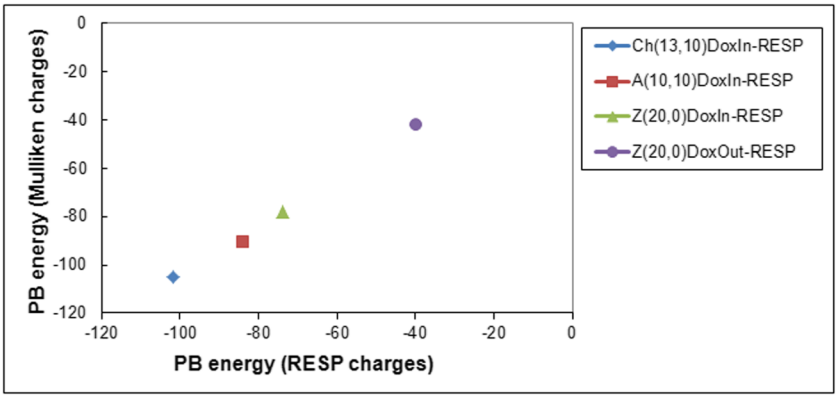

Fig. 5 Representation of the Poisson-Boltzmann (PB) binding-energies for DOX–CNT complexes obtained with the MM/PBSA method using DOX Mulliken charges vs. the corresponding values obtained using RESP charges (values in kcal/mol)

and their graphical comparison is depicted in Fig. S2. These results reinforce the validity of the qualitative trends found in this work indicating the ability of the nanotubes (ranking of reactivity) to adsorb or encapsulate DOX.

Together with the energy considerations, flattening of the nanotubes is observed for the DOX–CNT complexes with the strongest interaction, and the effect is diameter dependent. Ring A of the three planar rings of DOX (i.e., the farthest ring relative to the DOX-nitrogen atom) is stabilized at 3.58 to 3.98 Å from both internal nanotube walls, forming a kind of sandwich that can be interpreted as a double CNT–DOX–CNT π-π interaction, causing nanotube deformation from a circular to an elliptical shape. As an example of nanotube deformation, the nitrogen-doped *armchair* (10,10) nanotube, with PB value of − 109.8 kcal/mol and 14 Å diameter, is shown in Fig. 6 (run 2 of Table 1). The distance of the DOX-nitrogen atom to the nearest carbon atom of the nanotube sidewall ($d_{N\text{-}NT}$) remains 3.32 Å, smaller than $d_{p\text{-}NT}$, as in most encapsulation cases. In Fig. 7, the initial and final structures of some undoped systems (even with different chirality) indicate that those with the strongest interaction present larger nanotube deformation (*a* and *c* in Fig. 7, respectively, runs 1 and 14 in Table 1). For a better understanding of this flattening behavior, Table 1 presents representative distances between the planar section of DOX (hydroxyanthraquinone rings) and the nearest carbon atom of the opposite nanotube sidewall ($d'_{p\text{-}NT}$)—the other part of the sandwich.

A *chiral* (6,3) nanotube was reported as the *chiral* nanotube with the smallest diameter that allows DOX encapsulation, as determined by molecular dynamics simulations [32]. The diameter of the (6,3) nanotube is 6.17 Å, and DOX has approximate dimensions of 15 × 10.8 × 6.4 $Å^3$, which suggests an error in the value reported by Ghadamgahi and Ajloo [32]. In the present work, the molecular dynamics results for a *chiral* (10,7) nanotube, with a diameter of 11.51 Å, which barely allows DOX to enter the cavity, show a system where the repulsive forces make DOX exit the nanotube. The PB binding energy is − 71.4 kcal/mol, which is within the encapsulation energy range (Note that DOX structure is partially optimized in this case; the optimized structure used in all the other studied systems cannot be encapsulated in the (10,7) *chiral* nanotube). After extension of the molecular dynamics simulation to 8 ns, the drug retains half of its structure inside the nanotube due to π-stacking, with a final energy of − 72.5 kcal/mol. *Chiral* (12,9) nanotubes with diameters of 14 Å (and lengths of 33.9 Å) exhibit the strongest DOX–CNT molecular interaction with PB binding energies of − 85.9 and − 83.7 kcal/mol (runs 17 and 18, Table 2). Meanwhile *chiral* (13,10) nanotubes with larger diameters of 16.2 Å and lengths of 34.3 Å exhibit encapsulation PB

Table 3 The values of the binding energies for doxorubicin-nanotube complexes calculated using the Poisson-Boltzmann (PB) and Generalized Bond (GB) methods using RESP charges for doxorubicin. D is the nanotube diameter, $d_{p\text{-}NT}$ is the equilibrium distance between the doxorubicin planar fragment and the nanotube sidewall surface, $d'_{p\text{-}NT}$ is the equilibrium distance between the same point of the doxorubicin planar fragment and the opposite nanotube sidewall surface, and $d_{N\text{-}NT}$ is the equilibrium distance between the doxorubicin-nitrogen atom and the nanotube sidewall surface

Run	Type	PB (kcal/mol)	GB (kcal/mol)	D (Å)	Length (Å)	$d_{p\text{-}NT}$ (Å)	$d_{N\text{-}NT}$ (Å)	$d'_{p\text{-}NT}$ (Å)
1	A(10,10)DoxIn-RESP	− 100.3	− 103.3	14.03	20.22	3.656	3.336	4.714
2	Ch(13,10)DoxIn-RESP	− 101.8	− 105.3	15.50	18.33	3.817	3.248	3.926
3	Z(20,0)DoxIn-RESP	− 73.98	− 72.67	15.39	19.01	3.504	3.108	10.660
4	Z(20,0)DoxOut-RESP	− 37.73	− 35.76	15.39	19.01	3.340	4.748	–

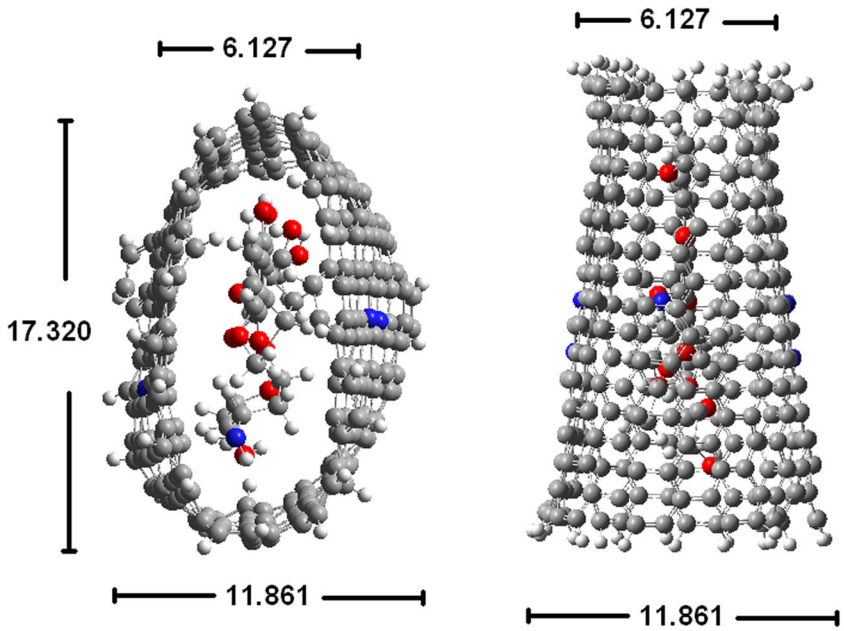

Fig. 6 Representation of the doxorubicin-nanotube complex for shorter nitrogen-doped *armchair* nanotubes, A(10,10)4NDoxIn, after AMBER simulations showing flattening of the nanotube and formation of a "nanotube sidewall-DOX-nanotube sidewall" sandwich due to double π-π stacking

binding energies of − 79.8 and − 81.2 kcal/mol for DOX positions v1 and v2 (please see definition below), respectively (runs 20 and 21, Table 2). The larger diameter *chiral* nanotubes do not favor DOX encapsulation, as indicated by the PB binding energy of − 65.4 kcal/mol (run 31, Table 2, diameter of 21.4 Å). The shorter nanotubes with diameters ~ 16 Å and lengths of 18.3 Å exhibit a PB binding energy of − 105.0 kcal/mol (run 14, Table 1 and Fig. 7c). The best DOX–CNT molecular interactions are exhibited by the 14 Å diameter *chiral* nanotube (− 110.6 kcal/mol, run 13, Table 1). In sum, the nanotube diameter is a more relevant parameter than the length, despite the fact that shorter nanotubes generally exhibit

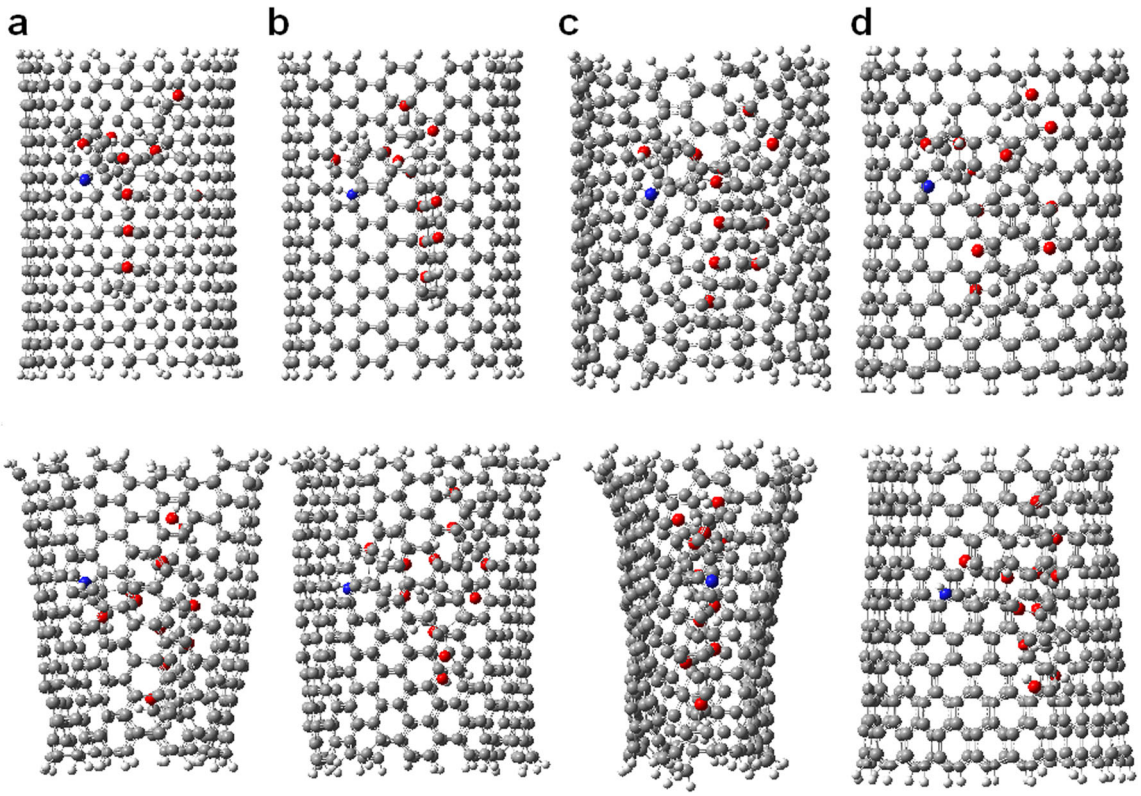

Fig. 7 Representation of the DOX encapsulation complexes formed with *armchair*, *chiral,* and *zigzag* nanotubes. **a** A(10,10)DoxIn; **b** A(12,12)DoxIn; **c** Ch(13,10)DoxIn; **d** Z(20,0)DoxIn, before and after the AMBER simulation (superior and inferior structures, respectively)

more favorable interactions with DOX. For longer or shorter nanotubes, *chiral* nanotubes exhibit the strongest DOX–CNT interactions, compared with *armchair* and *zigzag* nanotubes, when the diameter is 16 Å. At diameters of 14 Å, this trend is reversed, and DOX-*chiral* nanotubes exhibit the comparative weakest molecular interactions.

Therefore, if the diameter is very small, repulsive destabilizing forces are generated, which do not favor encapsulation. If the diameter is too large, DOX cannot form π-stacking interactions with both of the closer inner-wall sections of the nanotube, and significant nanotube deformation is not expected. Consequently, good stabilization of the complex does not occur. When the diameter enables more zones of reciprocal attraction to be formed, the resulting complex is more stable and the nanotube becomes flattened.

Additional results obtained with *zigzag* (30,0) nanotubes confirm the trends found. At higher diameter a lower DOX–CNT interaction is expected and indeed the *zigzag* (30,0) nanotubes of diameter ~ 24 Å show PB binding energies for DOX encapsulation of − 67.0 and − 69.1 kcal/mol for nanotubes of 21 and 34 Å length, respectively (run 12, Table 1 and run 39, Table 2) compared with PB binding energies of − 76.7 and − 108.5 kcal/mol for nanotubes of ~ 31–33 Å length and ~ 16 and ~ 14 Å diameter, respectively (run 35 and 32, Table 2). The length of the nanotube was not as decisive as the diameter. In addition, for this larger diameter (30,0) nanotube, greater equilibrium distances together with a slight nanotube deformation were observed, as expected. For (30,0) nanotube, the DOX adsorption energy of − 43.8 kcal/mol (run 38, Table 2) was significantly smaller than that of DOX encapsulation, as was also expected and in the same range of the DOX adsorption energy for smaller diameter nanotube (− 43.3 kcal/mol; ~ 16 Å diameter; run 34, Table 2).

Our results reveal that the important parameters that enhance the DOX–CNT interaction together with the nanotube diameter are those that facilitate the electrostatic interactions, such as the overall interaction of the three principal parts: the double π-π interaction of the planar DOX rings with the two pyrimidine rings of the nanotube and the interaction of the DOX-nitrogen atom with the nanotube sidewall surface (run 4 Table 2). A similar noncovalent interaction was found to play an essential role in explaining energetic behavior of a mepivacaine-*armchair* (5,5) single-walled CNT complex [45].

Doxorubicin position

The results in Table 2 reveal that complexes formed with encapsulated DOX in longer nanotubes are much more stable than those in which DOX is adsorbed on the outer surface of the nanotube. This finding is in agreement with the reported theoretical work on *armchair* nanotubes [31]. We found that this result holds for all systems formed by *zigzag*, *armchair*, and *chiral* nanotubes. PB binding energies for adsorbed doxorubicin between − 42.4 and − 43.3 kcal/mol are obtained for the *armchair*, *chiral* and *zigzag* nanotubes (runs 9, 19 and 34), in comparison with systems containing encapsulated DOX, with PB binding energy values smaller than − 73 kcal/mol. Therefore, encapsulated DOX forms complexes with stronger stabilizing interactions than adsorbed DOX, showing an increasing trend in the order of *zigzag* < *armchair* < *chiral* nanotubes, with PB binding energies of − 76.7, − 77.7, and − 81.2 kcal/mol, respectively (runs 35, 11 and 21).

The position of DOX inside the nanotube is defined as "v1" if its structure is located in such a way that its planar part, consisting of the three hydroxyanthraquinone rings, is oriented toward the outside end of the tube (i.e., if the fragment containing the DOX-nitrogen atom is oriented toward the center of the nanotube). The inverse position of DOX inside the nanotube is designated "v2". Figure 3a shows an example of DOX position v1 in *armchair* nanotube and Fig. 8 shows positions v1 and v2 of DOX encapsulated in *chiral* complexes with bumpy defects and four PEG fragments (with four ethylene glycol units each), before and after AMBER simulations. The regular nanotubes with larger diameters (16 Å) exhibit better interactions at position v2 (PB energies of − 77.7 and − 81.2 kcal/mol, runs 11 and 21, Table 2) than at the corresponding position v1 (runs 10 and 20). In contrast, the nanotubes with smaller diameters (14 Å) exhibit better interactions at position v1, with PB binding energies of − 109.3, − 85.9, and − 108.5 kcal/mol (runs 1, 17, and 32, Table 2, respectively), compared with − 89.7, − 83.7, and − 83.8 kcal/mol at position v2 (runs 2, 18, and 33). Nanotubes with smaller diameter exhibit stronger DOX–CNT interactions and are more sensitive to the DOX position, with an energy difference, for positions v1 and v2, greater than 19 kcal/mol. Meanwhile, the v1 and v2 energy differences for nanotubes with larger diameters are much smaller. To further investigate the effect of the initial relative position of DOX in relation to the nanotube, different dispositions of the two pyrimidine rings of doped nanotubes (located the same distance from the end) are considered (runs 3 and 4, Table 2, respectively, designated 4N and 4N'). The results are similar to those obtained for positions v1 and v2 in undoped systems (runs 1 and 2, Table 2). When DOX establishes an interaction with the tube host through two, or at best three, zones of attractive forces, the overall molecular interaction stabilizes the system, and no significant relative position changes occur, as observed for the system in run 4. When the production step is extended by a number of additional independent steps (multiple cycles from 2.1 to 40 ns), no significant final energy differences for each cycle are obtained, with final values of PB and GB of − 109.2 and − 113.8 kcal/mol, respectively. Note that standard deviations for most of the PB and GB energies are approximately 3 to 4 kcal/mol.

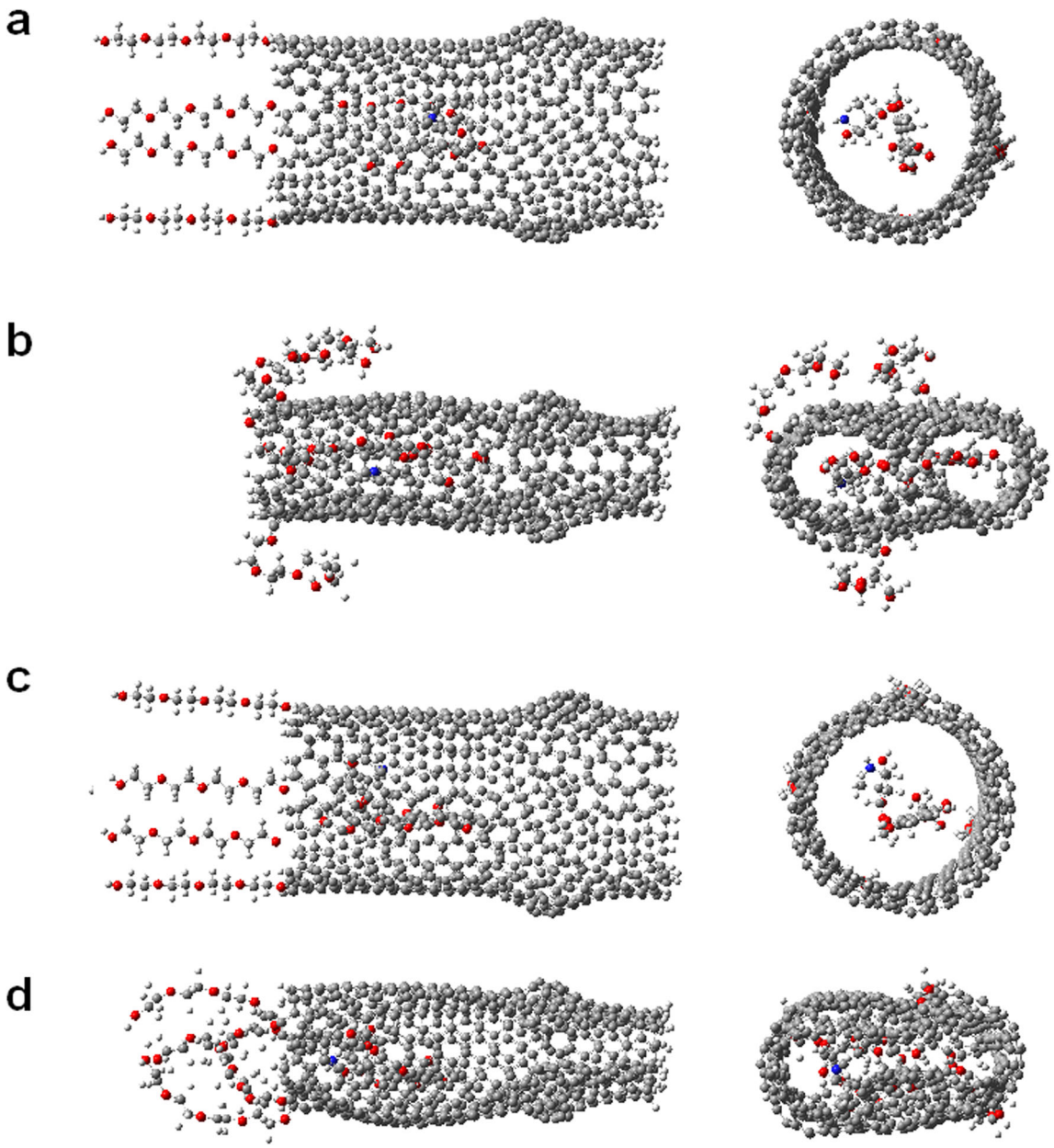

Fig. 8 Representation of the DOX–CNT encapsulation complexes Ch(13,10)BDoxR-4PEG4 with the drug located in the regular part of the nanotube containing bumpy defects and four PEG fragments. **a** and **b** represent DOX in position v1 before and after AMBER simulation, respectively. The figures **c** and **d** represent DOX in position v2 before and after AMBER simulation, respectively. Lateral views are on the left and frontal views are on the right

Bumpy defects and PEG

For regular nanotubes, the DOX–CNT interaction for encapsulation case is strongest when the molecular parameters principally favor π-π stacking (planar aromatic rings of doxorubicin interact, in a simple or double way, with one sidewall or both opposite sidewalls of the nanotube, respectively) and electrostatic interactions (through the DOX-nitrogen atom and the nanotube surface), which produces a flattening of the nanotube to improve the interaction with the DOX. With the aim of understanding the behavior of bumpy-defected nanotubes and the effect of PEG nanotube functionalization on DOX–CNT molecular interactions, a number of complexes are summarized in Table 2. The effect of bumpy-defected nanotubes depends on chirality. For *armchair* nanotubes, bumpy defects do not favor DOX–CNT interactions if the DOX is initially located near the defect (DoxD, runs 5, 6, 13, and 14) or if it is located in the regular part of the nanotube (DoxR, runs 7, 8, 15, and 16). Better interactions in these cases are exhibited by systems without bumpy defects. In contrast, for *chiral* nanotubes, bumpy defects favor DOX–CNT interactions with a clear dependence. Structures that

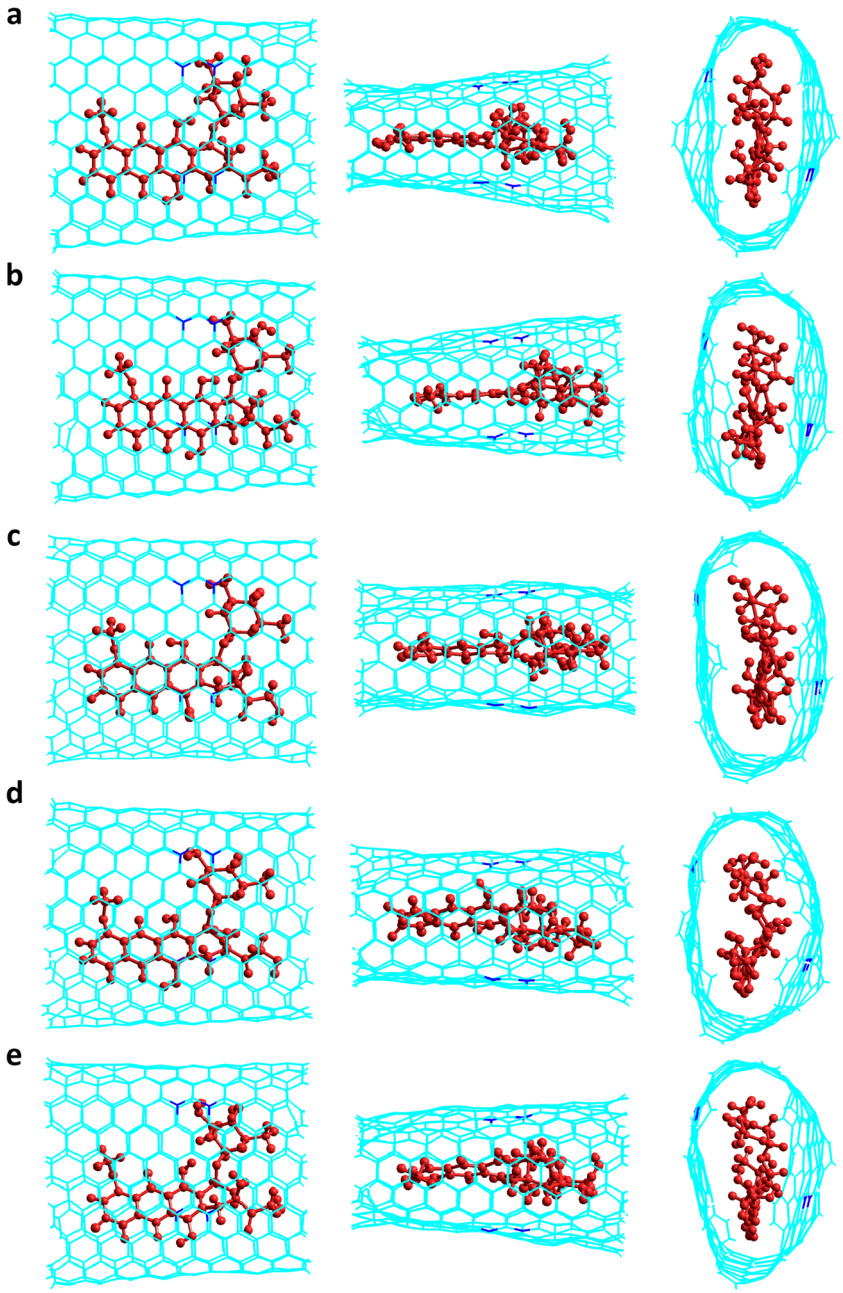

Fig. 9 Representation of the final structure of A(10,10)4NDoxIn complex, formed by DOX encapsulation in doped armchair nanotube, after a number of independent production steps of AMBER simulation at **a** 22.1 ns; **b** 47.1 ns; **c** 67.1 ns; **d** 82.1 ns, and **e** 100.6 ns. First two structures on the left are lateral views; frontal views are on the right

initially have DOX located in the regular part of the nanotube (DoxR, runs 23 and 24), exhibit the strongest interactions, with PB binding energies of − 94.2 and − 97.9 kcal/mol, compared to structures with the DOX initially located near the defect, with PB energies of − 84.1 and − 91.5 kcal/mol (DoxD, runs 25 and 26). The interactions are especially favored when the DOX is initially located in position v2 (runs 24 and 26).

The fact that PEG fragments enhance nanotube solubility requires that these fragments be located on the external surface of the nanotube, as shown in Fig. 8. PEG functionalization of *chiral* nanotubes constitutes an important contribution for longer nanotubes. It enables favorable DOX–CNT PB binding energies, with values of − 92.4 kcal/mol (run 27, Table 2), compared with the PB of − 81.2 kcal/mol for systems without PEG (run 21, Table 2). For shorter nanotubes, PEG functionalization is less significant, with a PB energy value of − 105.9 kcal/mol (run 18, Table 1), compared with a PB energy value of − 105.0 kcal/mol for nanotubes without PEG (run 14, Table 1). These are considered good results because PEG fragments enhance the complex solubility without negatively affecting the nanotube-drug interactions. The results suggest that the DOX–CNT interaction is stronger when two PEG fragments, each with eight units of ethylene glycol (run

18, Table 1, PB value of − 105.9 kcal/mol), are used instead of four fragments containing four ethylene glycol units each (run 17, Table 1, PB value of − 91.1 kcal/mol). Longer nanotube complexes exhibit a similar but less significant binding energy trend, as shown for Ch(13,10)BDoxR-2PEG8.v2, with PB energy of − 84.1 kcal/mol (run 28, Table 2), compared with Ch(13,10)BDoxR-4PEG4.v2, with PB energy of − 83.3 kcal/mol (run 30, Table 2).

Recently, MM/PBSA, one of the methods used in this work, was reported as a very successful method for ranking ligand-protein intermolecular interactions estimating their binding energies. The method was experimentally validated [46] confirming it as a useful tool for ranking ligand-receptor intermolecular interactions.

Final remarks

Among the factors to consider in order to improve the design of drug delivery systems (DDS) based on CNTs, it is very valuable and useful to know the non-covalent drug-nanotube attraction forces that occur in the adsorption of the drug. Through the knowledge of the way in which the molecular structure of the nanotube favors that interaction, it is possible to predict, as a first approximation, scales of relative reactivity of the nanotubes as drug receptors and provide necessary information to design DDS systems using CNTs with molecular structures that adsorb DOX more efficiently. That was one of the principal aims of this work.

It is also interesting to know the desorption energies of the drug, especially in acidic pH conditions in which this process actually occurs in most target areas. An approach to solve this point could be achieved by studying the behavior of the protonated drug against the different molecular structures of the nanotubes and their influence on the interaction energies between the protonated drug and the nanotube.

The present work has been focused exclusively on the comparative MD study of drug-nanotube non-covalent interactions considering a wide variety of both the structural characteristics of the nanotube, and the relative spatial dispositions of the drug in a neutral state, through the MM/PBSA and MM/GBSA methods. These methods, implemented in the AMBER programs [39], consider the ligand-receptor conjugate solvated by explicit solvent (in this case water in an octahedral box) and their validity has been demonstrated, for instance, in the prediction of an activity ranking in biological systems, experimentally corroborated [46].

In this work, the TIP3P water model has been used. Any DOX-water interaction is believed to affect in the same way every one of the studied systems so it was not taken in special consideration. To investigate if the calculations were dependent on the water model, simulations were made using a TIP4P water model reported to reproduce solvation free energies [47]; results exhibit no significant differences in the relative values of the drug-nanotube binding energies revealing the same tendency for both water models as depicted in Fig. S1.

As known, in molecular dynamics simulations, in addition to the appropriate force field and the choice of the box and type of solvent, sampling is an essential factor for obtaining reproducible and representative real interaction energy values (a list of the used additional parameters is included as supplementary material in Table S2). Experts [41] recommend running several short but independent simulations, rather than very long simulations for having better results and that was the preferred chosen procedure as was explained in methods section. However, for some systems, long production stages were also designed, which revealed, as expected, both PB (and GB) binding energy values and interaction geometries similar and showing no significant differences with those obtained with short simulations. For example, in the case of A(10,10)4NDoxIn system with a PB binding energy of − 109.8 kcal/mol (Table 1, run 2), by extending the simulation to 100 ns, by means of several independent simulation steps of 5 ns each one with all other parameters keep identical to the initial ones, a final value of − 109.9 kcal/mol was obtained with geometries depicted in Fig. 9 (and Table S3) revealing π-π stacking interactions and system stability (tip: natotube-nitrogen atoms can serve as reference points for comparing the complex structures). As another example, a sampling extension from 2 ns to 40 ns for the A(10,10)4N'DoxIn system (stoichiometry $C_{583}H_{69}N_5O_{11}$) with a PB binding energy of − 109.0 kcal/mol (Table 2, run 4) exhibits a PB binding energy of − 109.2 kcal/mol. These results confirm the advantage of using short independent simulations in the establishment of relative scales of drug-nanotube interaction energies for different nanotube structures through the MM/PBSA and MM/GBSA methods. In this way, it is demonstrated that reproducible activity ranking results can be obtained without using large amounts of computational resources.

Conclusions

The intermolecular interaction energies between the anticancer drug DOX and finite open and hydrogen-terminated single-walled CNT with different diameters, lengths and chirality were determined by MM/PBSA and MM/GBSA methods implemented in molecular dynamics program AMBER 12.

Our results reveal interesting reactivity trends such as (i) *armchair*, *zigzag* and *chiral* nanotubes 14 Å in diameter favor DOX–CNT complex formation and exhibit the optimal DOX–CNT interactions; (ii) the encapsulated DOX exhibit stronger DOX–CNT stabilizing interactions than the adsorbed DOX (in agreement with other authors); (iii) the nitrogen-doping effect and the presence of bumpy defects influence the DOX–CNT interactions in a chirality-dependent manner;

(iv) PEG functionalization of *chiral* nanotubes and the presence of bumpy defects favor interactions with DOX; (v) formation of a double π-π stacking of the DOX flat rings (interacting through both of its faces) with each of the two closer inner wall surfaces of the CNT is diameter dependent; and (vi) better DOX–CNT interactions involve a significant deformation or flattening of the nanotube.

Chiral, *zigzag*, and *armchair* nanotubes are promising drug-carrier structures, as are nitrogen-doped *armchair* and *zigzag* nanotubes, provided the adequate diameter and length are used. These results can be helpful in the molecular design of CNT as the framework of more efficient drug carriers.

Acknowledgments This work was partially supported by the Direction of Scientific and Technological Research DICYT-USACH Project Nr. 061641CF and by the Sociedad de Desarrollo Tecnológico SDT-USACH Project Nr. CIA 2981. We are also grateful for the allocation of computer time at the Chemistry and Biology Faculty cluster. We also thank Mr. Rodrigo Yañez for computer facilities.

Compliance with ethical standards

Conflict of interest The authors declare that they have no conflicts of interest.

References

1. Mehra NK, Jain K, Jain NK (2016) In: Grumezescu AM (ed) Nanobiomaterials in medical imaging. Oxford, Elsevier
2. Son KH, Hong JH, Lee JW (2016) Carbon nanotubes as cancer therapeutic carriers and mediators. Int J Nanomedicine 11:5163–5185
3. Liu Z, Tabakman SM, Chen Z, Dai H (2011) In: Klingeler R, Sim RB (eds) Carbon nanotubes for biomedical application. Springer-Verlag, Heidelberg
4. DeRosa AM, Greco K, Rajamani S, Sitharaman B (2010) Recent patents on single-walled carbon nanotubes for biomedical imaging, drug delivery and tissue regeneration. Rec Pat Biomed Eng 3:86–94
5. Mehra NK, Jain NK (2016) Multifunctional hybrid-carbon nanotubes: new horizon in drug delivery and targeting. J Drug Target 24:294–308
6. Prakash S, Malhotra M, Shao W, Tomaro-Duchesneau C, Abbasi S (2011) Polymeric nanohybrids and functionalized carbon nanotubes as drug delivery carriers for cancer therapy. Adv Drug Deliv Rev 63:1340–1351
7. Prato M, Kostarelos KAB (2008) Functionalized carbon nanotubes in drug design and discovery. Acc Chem Res 41:60–68
8. Dumortier H, Lacotte S, Pastorin G, Marega R, Wu W, Bonifazi D, Briand JP, Prato M, Muller S, Bianco A (2006) Functionalized carbon nanotubes are noncytotoxic and preserve the functionality of primary immune cells. Nano Lett 6:1522–1528
9. Madani SY, Tan A, Dwek M, Seifalian AM (2012) Functionalization of single-walled carbon nanotubes and their binding to cancer cells. Int J Nanomedicine 7:905–914
10. Chen H, Ma X, Li Z, Shi Q, Zheng W, Liu Y, Wang P (2012) Functionalization of single walled carbon nanotubes enables efficient intracellular delivery of siRNA targeting MDM2 to inhibit breast cancer cells growth. Biomed Pharmacother 66:334–338
11. Heister E, Neves V, Tîlmaciu C, Lipert K, Sanz Beltrán V, Coley H (2009) Triple functionalisation of single-walled carbon nanotubes with doxorubicin, a monoclonal antibody, and a fluorescent marker for targeted cancer therapy. Carbon 47:2152–2160
12. Beg S, Rizwan M, Sheikh AM, Hasnain MS, Anwer K, Kohli K (2011) Advancement in carbon nanotubes: basics, biomedical applications and toxicity. J Pharm Pharmacol 63:141–163
13. Nayak TR, Leow PC, Ee PLR, Arockiadoss T, Ramaprabhu S, Pastorin G (2010) Crucial parameters responsible for carbon nanotubes toxicity. Curr Nanosci 6:141–154
14. Wang L, Shi J, Zhang H, Li H, Gao Y, Wang Z, Wang H, Li L, Zhang C, Chen C, Zhang Z, Zhang Y (2013) Synergistic anticancer effect of RNAi and photothermal therapy mediated by functionalized single-walled carbon nanotubes. Biomaterials 34:262–274
15. Terrones M (2007) Synthesis toxicity and applications of doped carbon nanotubes. Acta Microsc 16:33–34
16. Chizari K, Deneuve A, Ersen O, Florea I, Liu Y, Edouard D, Janowska I, Begin D, Pham-Huu C (2012) Nitrogen-doped carbon nanotubes as a highly active metal-free catalyst for selective oxidation. ChemSusChem 5:102–108
17. Hu X, Zhou Z, Lin Q, Wu Y, Zhang Z (2011) High reactivity of metal-free nitrogen-doped carbon nanotube for the C–H activation. Chem Phys Lett 503:287–291
18. Gong KP, Du ZH, Xia ZH, Durstock M, Dai LM (2009) Nitrogen-doped carbon nanotube arrays with high electrocatalytic activity for oxygen reduction. Science 323:760–764
19. Contreras ML, Villarroel I, Rozas R (2016) Hydrogen physisorption energies for bumpy, saturated, nitrogen-doped single walled carbon nanotubes. Struct Chem 27:1479–1490
20. Contreras ML, Cortés-Arriagada D, Villarroel I, Alvarez J, Rozas R (2014) Evaluating the hydrogen chemisorption and physisorption energies for nitrogen-containing single-walled carbon nanotubes with different chiralities: a density functional theory study. Struct Chem 25:1045–1056
21. Contreras ML, Villarroel I, Rozas R (2015) How structural parameters affect the reactivity of saturated and non-saturated nitrogen-doped single-walled carbon nanotubes of different chiralities: a density functional theory approach. Struct Chem 26:761–771
22. Zhang XK, Meng LJ, Lu QH, Fei ZF, Dyson PJ (2009) Targeted delivery and controlled release of doxorubicin to cancer cells using modified single wall carbon nanotubes. Biomaterials 30:6041–6047
23. Rodríguez-Galván A, Amelines-Sarria O, Rivera M, Carreón-Castro MP, Basiuk VA (2016) Adsorption and self-assembly of anticancer antibiotic doxorubicin on single-walled carbon nanotubes. Nano 11:1650038
24. Liang PC, Chen YC, Chiang CF, Mo LR, Wei SY, Hsieh WY, Lin WL (2016) Doxorubicin-modified magnetic nanoparticles as a drug delivery system for magnetic resonance imaging-monitoring magnet-enhancing tumor chemotherapy. Int J Nanomedicine 11:2021–2037
25. Fan X, Wang L, Guo Y, Xiong X, Zhu L, Fang K (2016) Inhibition of prostate cancer growth using doxorubicin assisted by ultrasound-targeted nanobubble destruction. Int J Nanomedicine 11:3585–3596
26. Ferreira DS, Faria SD, Lopes SCA, Teixeira CS, Malachias A, Magalhães-Paniago R, de Souza Filho JD, Oliveira BL, Guimarães AR, Caravan P, Ferreira LAM, Alves RJ, Oliveira MC (2016) Development of a bone-targeted pH-sensitive liposomal formulation containing doxorubicin: physicochemical characterization, cytotoxicity, and biodistribution evaluation in a mouse model of bone metastasis. Int J Nanomedicine 11:3737–3751
27. Meng L, Zhang X, Lu Q, Fei Z, Dyson PJ (2012) Single walled carbon nanotubes as drug delivery vehicles: targeting doxorubicin to tumors. Biomaterials 33:1689–1698
28. Carvalho C, Santos RX, Cardoso S, Correia S, Oliveira PJ, Santos MS, Moreira PI (2009) Doxorubicin: the good, the bad and the ugly effect. Curr Med Chem 16:3267–3285

29. Etheridge ML, Campbell SA, Erdman AG, Haynes CL, Wolf SM, McCullough J (2013) The big picture on nanomedicine: the state of investigational and approved nanomedicine products. Nanomed Nanotechnol Biol Med 9:1–14
30. Liu Z, Fan AC, Rakhra K, Sherlock S, Goodwin A, Chen X, Yang Q, Felsher DW, Dai H (2009) Supramolecular stacking of doxorubicin on carbon nanotubes for in vivo cancer therapy. Angew Chem Int Ed Engl 48:7668–7672
31. Wang Y, Xu Z (2016) Interaction mechanism of doxorubicin and SWCNT: protonation and diameter effects on drug loading and releasing. RSC Adv 6:314–322
32. Ghadamgahi M, Ajloo D (2015) Correlation of drug and carbon nanotube size in encapsulation and free energy calculation: a molecular insight. Bull Kor Chem Soc 36:168–179
33. Izadyar A, Farhadian N, Chenarani N (2015) Molecular dynamics simulation of doxorubicin adsorption on a bundle of functionalized CNT. J Biomol Struct Dyn 24:1–9. https://doi.org/10.1080/07391102.2015.1092475
34. Sommee P, Rungrotmongkol T, Saengsawang O, Arsawang U, Remsungnen T, Hannongbua S (2011) Understanding the molecular properties of doxorubicin filling inside and wrapping outside single-walled carbon nanotubes. J Comput Theor Nanosci 8:1385–1391
35. Chico L, Crespi VH, Benedict LX, Louie SG, Cohen ML (1996) Pure carbon nanoscale devices: nanotube heterojunctions. Phys Rev Lett 76:971–974
36. Stenberg M, Curtiss LA, Gruen DM, Kedziora G, Horner DA, Redfern PC, Zapol P (2006) Carbon ad-dimer defects in carbon nanotubes. Phys Rev Lett 96:75506
37. Contreras ML, Avila D, Alvarez J, Rozas R (2012) Computational algorithms for a fast building of 3D carbon nanotube models having different defects. J Mol Graph Mod 38:389–395
38. HyperChem release 7.5 Hypercube Inc 1115 NW 4th Street Gainesville Florida 32601 USA
39. Case DA, Cheatham III TE, Darden T, Gohlke H, Luo R, Merz Jr KM, Onufrie A, Simmerling C, Wang B, Woods R (2005) The Amber biomolecular simulation programs. J Comput Chem 26:1668–1688
40. Bayly CI, Cieplak P, Cornell W, Kollman PA (1993) A well-behaved electrostatic potential based method using charge restraints for deriving atomic charges: the RESP model. J Phys Chem 97:10269–10280
41. Genheden S, Ryde U (2015) The MM/PBSA and MM/GBSA methods to estimate ligand-binding affinities. Expert Opin Drug Discov 10:449–461
42. Liu Z, Tabakman S, Welsher K, Dai H (2009) Carbon nanotubes in biology and medicine: in vitro and in vivo detection, imaging and drug delivery. Nano Res 2:85–120
43. Liu Z, Sun X, Nakayama-Ratchford N, Dai H (2007) Supramolecular chemistry on water-soluble carbon nanotubes for drug loading and delivery. ACS Nano 1:50–56
44. Johnson ER, Keinan S, Mori-Sánchez P, Contreras-García J, Cohen AJ, Yang W (2010) Revealing noncovalent interactions. J Am Chem Soc 132:6498–6506
45. Beyramabadi SA, Khadivjam T, Gonabadi A, Morsali A, Gharib A, Khashi M, Khorsandi-Chenarboo M (2017) A DFT study on the geometry, tautomerism and noncovalent interactions of the Mepivacaine drug with the pristine SWCNT and –COOH functionalized SWCNT. J Theor Comput Chem. 16:1750008 [16 pages]. https://doi.org/10.1142/S0219633617500080
46. Westermaier Y, Ruiz-Carmona S, Theret I, Perron-Sierra F, Poissonnet G, Dacquet C, Boutin JA, Ducrot P, Barril X (2017) Binding mode prediction and MD/MMPBSA-based free energy ranking for agonists of REV-ERBα/NCoR. J Comput Aided Mol Des. https://doi.org/10.1007/s10822-017-0040-7
47. Nerenberg PS, Jo B, So C, Tripathy A, Head-Gordon T (2012) Optimizing solute-water van der Waals interactions to reproduce solvation free energies. J Phys Chem B 116(15):4524–4534